

University of Nebraska - Lincoln
DigitalCommons@University of Nebraska - Lincoln

Mechanical & Materials Engineering Faculty
Publications

Mechanical & Materials Engineering, Department
of

2016

Pulsed Laser Cutting of Magnesium-Calcium for Biodegradable Stents

M. P. Sealy

University of Nebraska-Lincoln, sealy@unl.edu

Y. B. Guo

University of Alabama - Tuscaloosa, yguo@eng.ua.edu


J. F. Liu

University of Alabama - Tuscaloosa

C. Li

University of Alabama - Tuscaloosa

Follow this and additional works at: <http://digitalcommons.unl.edu/mechengfacpub>

 Part of the [Mechanics of Materials Commons](#), [Nanoscience and Nanotechnology Commons](#), [Other Engineering Science and Materials Commons](#), and the [Other Mechanical Engineering Commons](#)

Sealy, M. P.; Guo, Y. B.; Liu, J. F.; and Li, C., "Pulsed Laser Cutting of Magnesium-Calcium for Biodegradable Stents" (2016).
Mechanical & Materials Engineering Faculty Publications. 261.
<http://digitalcommons.unl.edu/mechengfacpub/261>

This Article is brought to you for free and open access by the Mechanical & Materials Engineering, Department of at DigitalCommons@University of Nebraska - Lincoln. It has been accepted for inclusion in Mechanical & Materials Engineering Faculty Publications by an authorized administrator of DigitalCommons@University of Nebraska - Lincoln.

18th CIRP Conference on Electro Physical and Chemical Machining (ISEM XVIII)

Pulsed Laser Cutting of Magnesium-Calcium for Biodegradable Stents

M.P. Sealy^a, Y.B. Guo^{b*}, J.F. Liu^b, C. Li^b

^aDept. of Mechanical and Materials Engineering, University of Nebraska-Lincoln, W342 Nebraska Hall, Lincoln, NE 68588, U.S.A.

^bDept. of Mechanical Engineering, The University of Alabama, 359 H.M. Comer Hall, Tuscaloosa, AL 35401, U.S.A.

* Corresponding author. Tel.: +1-205-348-2615; fax: +1-205-348-6419. E-mail address: yguo@eng.ua.edu

Abstract

There is growing interests in the use of biodegradable magnesium implants for cardiovascular and pulmonary applications such as stents. Magnesium is a metal that has the ability to gradually dissolve and absorb into the human body after implantation. There is very little work discussing the relationship between process parameters and cut quality of magnesium stents by laser cutting. The objective of this research is to determine the effect of laser cutting conditions including peak laser power and cutting speed of a millisecond range pulsed laser on kerf geometry, surface topography, surface roughness, and microstructure. An assessment on the experimental work discussing laser cutting of magnesium alloys is also presented.

© 2016 The Authors. Published by Elsevier B.V. This is an open access article under the CC BY-NC-ND license (<http://creativecommons.org/licenses/by-nc-nd/4.0/>).

Peer-review under responsibility of the organizing committee of 18th CIRP Conference on Electro Physical and Chemical Machining (ISEM XVIII)

Keywords: Laser cutting; surface integrity; magnesium; stent; biodegradable implant

1. Introduction

There is growing interests in the use of biodegradable implants for cardiovascular and pulmonary applications such as stents. Current commercially available degradable polymers (e.g. PLLA) have inferior mechanical properties compared to a permanent metal device. An alternative degradable biomaterial is a magnesium alloy. Magnesium is a metal that has the ability to gradually dissolve and absorb into the human body after implantation. Full degradation of a magnesium stent can occur in a few months.

While several studies have shown that magnesium stents have proven successful in human clinical trials [1-4], there is little work in literature discussing the manufacturing process mechanisms and its relationship with cut quality. Stents are fabricated by precision laser cutting the intricate geometrical pattern that constitutes the stent's design. The critical technical challenge is that laser cutting can induce thermal damage that negatively affects corrosion mechanisms *in vivo*. Thermal damage in the form of a heat affected zone (HAZ), micro-cracks, or tensile residual stress can further accelerate corrosion rates. Therefore, it is important to understand how process parameters influence the resulting surface integrity.

In this study, a design-of-experiment (DOE) approach that characterized the effects of process parameters, i.e. laser power and cutting speed, was investigated. The objective was to better understand how process parameters influence cut quality after laser cutting a magnesium alloy. The effects of cutting speed and peak power while maintaining a fixed average power on the resulting kerf geometry, topography, surface roughness, and microstructure were investigated.

Nomenclature

P_{peak}	peak pulse laser power (W)
P_{avg}	average laser power (W)
v	cutting speed (mm/min)
τ	pulse width (s)
f	frequency (Hz)
θ	taper angle
d_{entry}	entry kerf width (μm)
d_{exit}	exit kerf width (μm)
h	sample thickness (μm)

2. Laser cutting of a magnesium alloy

2.1. Cutting mode and pulse width

Demir and Previtali investigated the influence of (a) cutting mode, i.e. continuous wave (CW) versus pulsed, and (b) pulse width, i.e. nanosecond versus femtosecond, in order to help establish a benchmark in machining quality, productivity, and ease of processing [5]. In CW mode, the laser was a YLR-150-750-QCW from IPG Photonics. In pulsed mode, the nanosecond laser was a Q-switched active fiber laser (YLP-1/100/50/50) from IPG Photonics, and the femtosecond laser was a StarFemto system from Rofin-Baasel Lasertechnik. The pulse widths were 250 ns and 800 fs. The spot size ranged from 22 μm to 32 μm depending on the laser system. The max peak power (max average power) for the CW, ns, and fs laser systems was 250 W (250 W), 9 kW (50 W), and 60 MW (6 W), respectively. Dross was removed by chemical etching in ethanol-HNO₃.

The cutting conditions in CW mode were 150 W laser power and a 1200 mm/min cutting speed. The laser was focused at the kerf exit in order to allow for the highest irradiance. The sample was a 0.4 mm thick sheet of AZ31. N₂ was used as a shielding gas to prevent oxidation. For ns pulse width cutting, the average power was 7.5 W, the cutting speed was 120 mm/min, and the frequency was 25 kHz. These conditions were chosen so that the laser would not damage the backside of the AZ31 tube (0.2 mm thick; 2.5 mm dia.). For femtosecond cutting, the average power was 5 W, the cutting speed was 300 mm/min, and the frequency was 200 kHz. For both pulsed laser, argon was used a shielding gas.

Similar to other results widely published in literature for different materials, the investigators showed that ultrashort pulsed lasers produce a higher cut quality. The resulting kerf widths and cutting edges are shown in Fig. 1. The kerf was relatively straight for the CW laser. The ns pulsed lasers tended to have larger taper angles. The dross height for a CW laser was as high as 185 μm . For ns pulsed laser, dross was approximately 85 μm . The fs pulsed laser had minimal dross. The corresponding surface roughness (R_z) for CW, ns-pulsed, and fs-pulsed laser was 6.1 μm , 4.6 μm , and 1.4 μm .

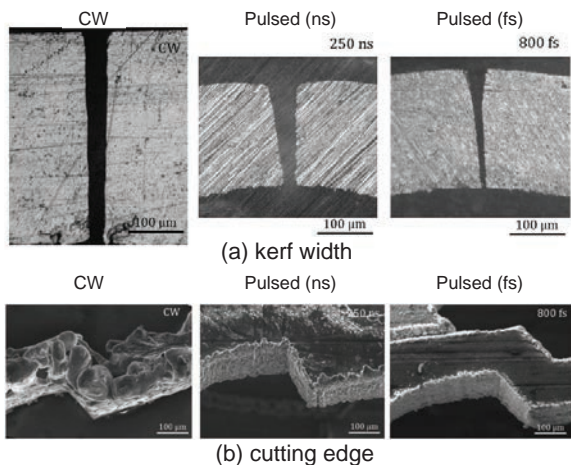


Fig. 1 Laser cutting AZ31 with a CW laser, nanosecond pulsed laser, and femtosecond pulsed laser [5].

Interestingly, the investigators compared the complete cycle time to fabricate a stent by each laser. The cycle time included cutting, etching, and cleaning times. They showed that even though the pulsed lasers had longer cutting times than the CW laser, a stent cut using a pulsed laser still had a shorter cycle time since less post-processing like etching and cleaning were needed. A CW laser cut surface had a higher amount of melt deposit that was more difficult to remove. Therefore, the advantage of using a higher cutting speed (1200 mm/min) with a CW laser did not translate into higher productivity.

Furthermore, the authors showed that even though a femtosecond pulsed laser did not eliminate the need for post-processing, the cycle time was reduced approximately 40%. The authors also acknowledged that the higher cost of a femtosecond laser may be cost prohibitive for some industries. A ms pulsed laser may provide a more balanced tradeoff between cutting time and cut quality.

2.2. Assist gas

Demir *et al.* investigated the surface quality after laser cutting AZ31 tubes with a Q-switched, nanosecond pulsed fiber laser that had a 23 μm spot size [6, 7]. The average laser power was 5 W and the cutting speed was 120 mm/min. The investigators compared cutting in an inert gas environment using argon gas to cutting in a reactive environment by using oxygen gas. Although the kerf was clearly open, a significant amount of dross formed on the top surface when cutting with argon, see Fig. 2a. The investigators showed that chemical etching after argon assisted cutting significantly improved the geometrical integrity and surface finish. The surface roughness decreased more than 11%. The stent cut with oxygen showed less dross on the surface, but the kerf was not uniformly cut (Fig. 2b).

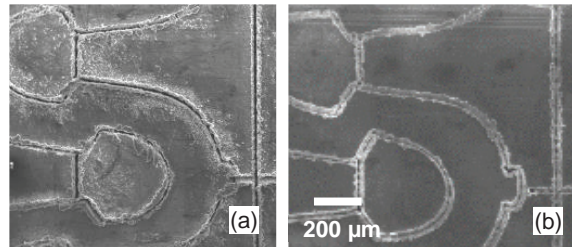


Fig. 2 Nanosecond pulsed fiber laser cutting of AZ31 tubes using (a) argon gas and (b) oxygen gas (Modified from [6]).

Fushimi *et al.* investigated the effect of varying gas pressure of a lower nozzle and the advantage of adding a secondary lower nozzle; see Fig. 3 [8]. The authors used a high energy CO₂ laser where the power was 1000 W, and the cutting speed was 1000 mm/min. The cut surfaces are shown in Fig. 4. Without assist gas, the dross height was reported as 1 mm, and no striations were observable. Dross free cuts were observed once the pressure reached 0.12 MPa. Further increasing the pressure caused dross to occur on top of the sample. The authors stipulate that when using a single nozzle, it must be in the direction of the cut. When two nozzles were introduced, dross free cutting was also obtained. The authors mention that dual nozzles may be a more effective approach when cutting more

complex geometries instead of using a single lower nozzle that could continuously require rotation.

Scintilla and Tricarico compared using two different gas pressure for a fiber and CO₂ laser source in continuous mode when cutting 1 mm thick AZ31 sheets [9]. Interestingly, the results showed that increasing the gas pressure from 0.3 MPa to 0.6 MPa caused the surface roughness to increase for the CO₂ laser and had a negligible effect for a fiber laser.

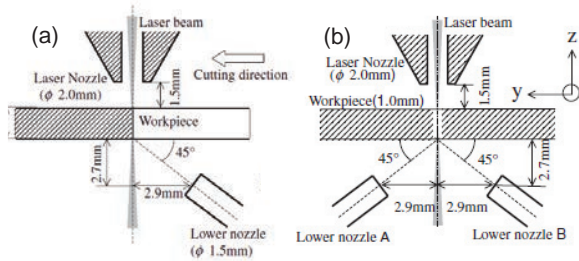


Fig. 3 Schematic of laser cutting with (a) single lower nozzle and (b) dual lower nozzles [8].

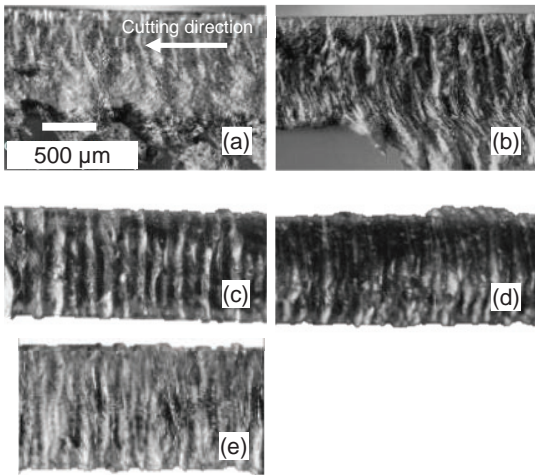


Fig. 4 CO₂ laser cutting of 1 mm thick AZ31 with (a) no assist gas and with N₂ as an assist gas at (b) 0.05 MPa (relative pressure to ambient pressure), (c) 0.12 MPa, (d) 0.19 MPa, and (e) dual nozzle configuration [8].

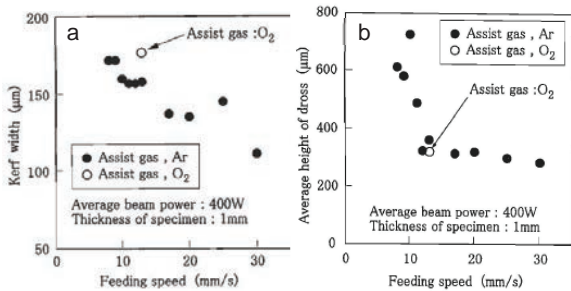


Fig. 5 Effect of cutting speed on the (a) kerf width and (b) average dross height from CO₂ laser cutting AZ31 [10].

2.3. Cutting speed

Shigematsu et al. investigated the effect of cutting speed on kerf width and average dross height using a CO₂ laser on AZ31, see Fig. 5 [10]. The average power was 400 W, and the cutting speed ranged from 480 mm/min to 1800 mm/min. The kerf width and average dross height declined as the cutting speed increased.

2.4. Laser type

Scintilla and Tricarico compared a fiber and CO₂ laser source in continuous mode when cutting 1 mm thick AZ31 sheets [9]. Argon was used as an assist gas. The laser power of the fiber and CO₂ lasers were 2 kW and 4 kW, respectively. The authors did not indicate the reason for choosing the maximum output power for each laser. The cutting speed was between 10,000 mm/min to 30,000 mm/min. The morphology of surface cut by the CO₂ laser exhibited inclined striations along the entire cutting edge [9]. For the fiber laser, the inclined striations were mostly confined to the lower half of the cut surface. The CO₂ laser produced a higher roughness than the fiber laser. Also, the dross height for the fiber laser was smaller than the CO₂ laser at lower cutting speeds. The authors concluded that fiber laser cutting had a higher quality cutting edge over a CO₂ laser.

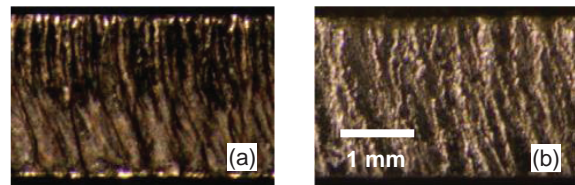


Fig. 6 Cut morphology after (a) fiber and (b) CO₂ laser cutting of AZ31. Modified from [9].

3. Experiment

3.1. Work material

In the following study, magnesium (Mg) was alloyed with 0.8 wt-% calcium (Ca). The alloy MgCa0.8 (referred to as MgCa) was prepared using pure Mg of ASTM grade 9980A and Mg-30%Ca master alloy. The pure Mg was melted down at 650 °C. Next, the melt was heated to 710 °C and Mg-30%Ca was added until reaching the target composition. The alloy was cast into ingots that were turned at 900 RPM without coolant into a 38.1 mm diameter round stock. The bar stock was further turned to cut 1 mm thick disks that were rolled to a final thickness of approximately 700 μm.

3.2. Fiber laser cutting

Laser cutting was performed using an ytterbium fiber laser from IPG Photonics (Model YLR-150/1500-QCW-MM-AC-Y11). The maximum average and peak powers were 150 W and 1500 W, respectively. The pulse width ranged from 0.2 ms to 50 ms. The wavelength was 1070 nm.

Argon was used as an assist gas. The purpose of the assist gas was to aid in removing molten material from the cut. It also shielded the cut from oxidation. The pressure was 120 psi. The nozzle diameter was 0.5 mm. The laser was focused on the sample surface and the standoff distance was 1 mm. The frequency was 1000 Hz and was selected based on preliminary testing to determine optimum pulse frequency.

Detailed laser cutting conditions are presented in Table 1. The experiment plan was designed to determine the effect of laser power and cutting speed on the resulting kerf width, taper angle, topography, surface roughness, and microstructure. Four levels for peak power and cutting speed were investigated. The pulse width was adjusted so that the average power remained a constant 150 W. The peak power is calculated based on Eqn. 1. The corresponding energy per pulse was 0.150 J. The spot diameter was approximately 72 μm corresponding to an energy density of 3684 J/cm^2 .

$$P_{peak} = \frac{P_{avg}}{\tau \cdot f} \quad (1)$$

Table 1. Fiber laser cutting conditions.

Exp. No.	Peak Power, P_{peak} (W)	Cutting Speed, v (mm/min)	Pulse Width, τ (ms)
1	1500	100	0.100
2	1500	400	0.100
3	1500	700	0.100
4	1500	1000	0.100
5	1200	100	0.125
6	1200	400	0.125
7	1200	700	0.125
8	1200	1000	0.125
9	900	100	0.167
10	900	400	0.167
11	900	700	0.167
12	900	1000	0.167
13	600	100	0.250
14	600	400	0.250
15	600	700	0.250
16	600	1000	0.250
17	300	100	0.500
18	300	400	0.500
19	300	700	0.500
20	300	1000	0.500

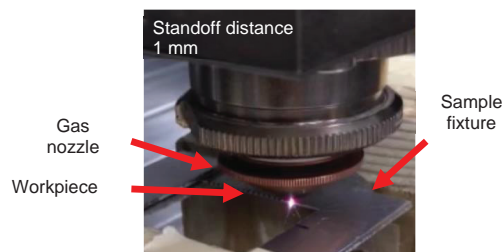


Fig. 7 Fiber laser cutting of MgCa.

4. Results

4.1. Kerf geometry

The laser cut MgCa samples were mounted in epoxy and polished by sand paper and subsequent oil-based diamond suspension up to 0.25 μm finish. The kerf profiles were characterized by KeyenceVHX-1000 digital optical microscope. To minimize error, kerf measurements were repeated three times along the cutting direction.

Fig. 8 shows a representative kerf profile of laser cut MgCa. The non-uniform kerf geometry can be characterized by entry kerf width, exit kerf width, and taper angle. The taper angle (θ) is given by:

$$\theta = \tan^{-1} \frac{d_{entry} - d_{exit}}{2h} \quad (2)$$

where d_{entry} and d_{exit} represent the entry kerf width and exit kerf width, respectively, and h is sample thickness.

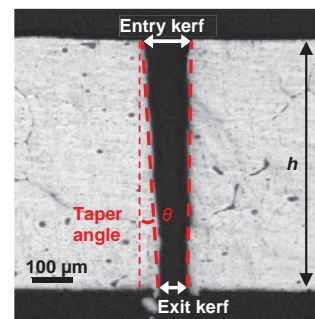


Fig. 8 Representative kerf geometry in laser cutting.

Fig. 9 shows the average entry kerf width as a function of cutting speed and peak power. At a low cutting speed ($v < 700$ mm/min), the entry kerf width generally decreased when decreasing peak power. At a high cutting speed ($v = 1000$ mm/min), the entry kerf width was less dependent on peak power. Moreover, at a constant peak power, the entry kerf was independent of the cutting speed.

Fig. 10 shows the average exit kerf width as a function of peak power and cutting speed. Similar to the entry kerf width at a low cutting speed ($v < 700$ mm/min), the exit kerf width also decreased by reducing the peak power from 1500 W to 600 W. However, the exit kerf width rebounded to a higher value once the power was further decreased to 300 W. This was because a minimum recast layer formed on the surface at the lowest peak power and therefore resulted in a wider exit kerf. More details regarding the recast layer will be discussed in section 4.4. On the contrary, at a high cutting speed ($v = 1000$ mm/min), the exit kerf width increased by decreasing peak power, which is also attributed to the reduction of a recast layer at low peak power.

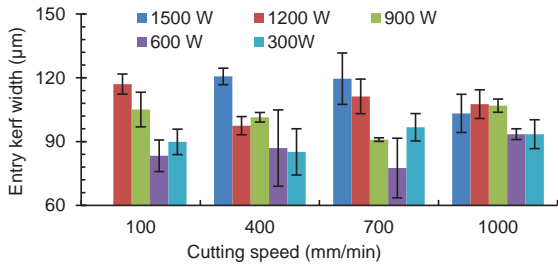


Fig. 9 Entry kerf width as a function of peak power and cutting speed.

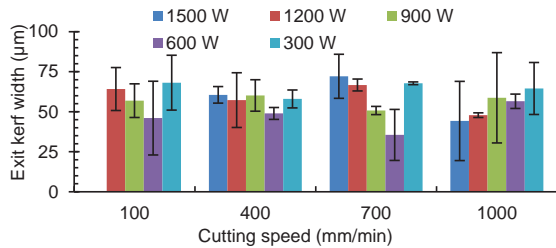


Fig. 10 Exit kerf width as a function of peak power and cutting speed.

Among all the cases, the average exit kerf width was always smaller than the average entry kerf width. This is because laser intensity degrades with the increase of penetration depth, and therefore, less material is ablated away near the exit kerf.

Fig. 11(a) shows the average taper angle ranging from 0° to 3° at different laser cutting conditions. At a constant cutting speed, a higher peak power usually resulted in a larger taper angle and indicated a non-uniform kerf profile. By decreasing the peak power from 1500 W to 600 W, the taper angle dropped below 1°, showing a relatively uniform kerf. In addition, a few negative error bars are observed in Fig. 11(a). The negative taper angle indicates the exit kerf was wider than the entry kerf. In a special case shown in Fig. 11(b), the kerf shows a hyperbolic characteristic instead of a taper profile. This may be attributed to the non-uniform distribution of the recast layer. Considering the irregular profile, more parameters (central kerf width, curvature etc.) will be used to characterize the kerf geometry in the future.

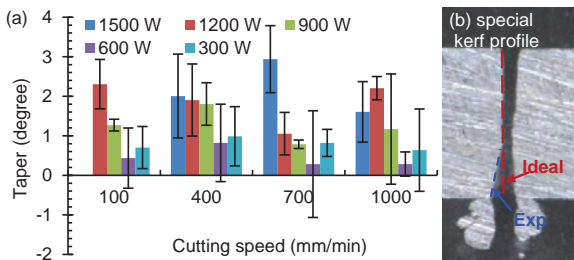


Fig. 11 (a) Taper angle as a function of peak power and cutting speed and (b) sample kerf profile.

4.2. Surface topography

Surface topography characteristics of laser cut samples were observed using a JEOL 7000 FE scanning electron microscope (SEM). Fig. 12 shows the representative surface topography varying with cutting speed and peak power. At a low peak power of 300 W, the surface morphology was independent of the cutting speed. Similar striations can be found on the surface regardless of changing cutting speed. A wavy pattern was observed in the striation as the result of molten material flow. No columnar micro-grooves were found on the surface. However, at a high peak power of 1200 W, the surface characteristic changed with the cutting speed. The wavy pattern evolved to a columnar micro-groove when increasing the cutting speed from 400 mm/min to 1200 mm/min.

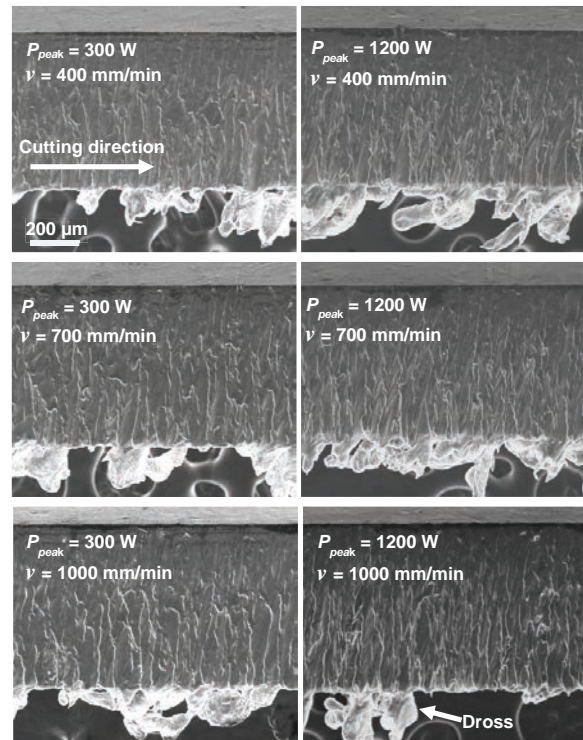


Fig. 12 Surface topography varying with cutting speed (v) and peak power (P_{peak}).

4.3. Surface roughness

Surface roughness (R_a) was measured along the laser cutting direction using a profilometer with a sampling length of 1 mm. Each sample was measured three times at different surface areas to minimize measurement error. Fig. 13 shows the average surface roughness at different cutting speeds and peak powers. Generally, surface roughness decreased with a reduction in peak power. R_a was independent of cutting speed. At a high peak power (900 W, 1200 W and 1500 W), the average roughness primarily ranged between 4 µm to 6 µm. At a low peak power (300 W and 600 W), R_a can be reduced to 2 µm to 3 µm. The reduction of surface roughness at low peak

powers can be attributed to the minimum recast layer formation.

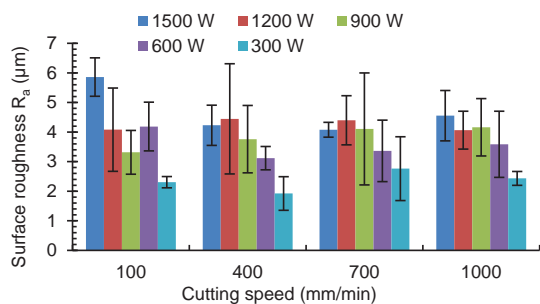


Fig. 13 Surface roughness as a function of peak power and cutting speed

4.4. Microstructure

The microstructure after laser cutting MgCa is shown in Fig. 14. To observe the microstructure, the polished samples were (1) etched by acetic glycol for approximately 5 sec (20 mL $C_2H_4O_2$ + 1 mL HNO_3 + 60 mL $C_2H_6O_2$ + 20 mL H_2O), (2) rinsed in water, and (3) ultrasonically cleaned in ethanol. One observable trend was that for a constant peak power, the thickness of the recast layer increased as the cutting speed increased. Another observable trend was that for a fixed cutting speed, the thickness of the recast layer increased with a higher peak power. More microcracks were observed at higher peak powers.

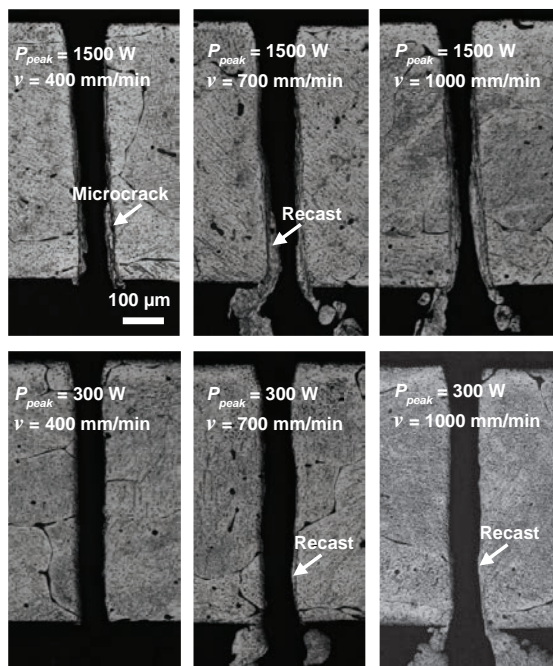


Fig. 14 Evolution of the recast layer with peak power and cutting speed.

5. Conclusions

Pulsed fiber laser cutting of MgCa with a millisecond range pulse width was performed to investigate the cut quality after increasing peak laser power and cutting speed. Kerf geometry, surface topography, surface roughness, and microstructure were measured. The process space for optimal cut quality may be found via an analysis of the effect size in a future study. In this work, the results indicated that:

- For the same energy input, lower laser powers had smaller taper angles due to less thermal damage
- Lower laser powers were less likely to have a columnar striations on the surface
- Lower powers tended to have a lower roughness while there was no trend observed with cutting speed.
- Low power and low speed tended to have thinner recast layer.

References

- [1] Di Mario C, Griffiths H, Goktekin O, Peeters N, Verbist J, Bosiers M, Deloose K, Heublein B, Rohde R, Kasese V, Ilesley C, Erbel R. Drug-eluting bioabsorbable magnesium stent. *J. Interv. Cardiol.* 2004; 17(6):391-395.
- [2] Erbel R, Di Mario C, Bartunek J, Bonnier J, de Bruyne B, Eberli FR, Erne P, Haude M, Heublein B, Horrigan M, Ilesley C, Böse D, Koolen J, Lüscher TF, Weissman N, Waksman R. Temporary scaffolding of coronary arteries with bioabsorbable magnesium stents: a prospective, non-randomised multicentre trial. *The Lancet.* 2007; 369(9576):1869-1875.
- [3] Peeters P, Bosiers M, Verbist J, Deloose K, Heublein B. Preliminary results after application of absorbable metal stents in patients with critical limb ischemia. *J Endovasc Ther.* 2005; 12(1):1-5.
- [4] Zartner P, Cesnjevar R, Singer H, Weyand M. First successful implantation of a biodegradable metal stent into the left pulmonary artery of a preterm baby. *Catheterization and Cardiovascular Interventions.* 2005; 66(4):590-594.
- [5] Demir AG, Previtali B. Comparative study of CW, nanosecond- and femtosecond-pulsed laser microcutting of AZ31 magnesium alloy stents. *Biointerphases.* 2014; 9(2):029004:1-10.
- [6] Demir AG, Previtali B, Colombo D, Ge Q, Vedani M, Petrini L, Wu W, Biffi CA. Fiber laser micromachining of magnesium alloy tubes for biocompatible and biodegradable cardiovascular stents. *Proc SPIE 8237, Fiber Lasers IX: Technology, Systems, and Applications.* 2012; 823730.
- [7] Demir AG, Previtali B, Biffi CA. Fibre laser cutting and chemical etching of AZ31 for manufacturing biodegradable stents. *Advances in Materials Science and Engineering.* 2013; 1-11.
- [8] Fushimi T, Kitazawa M, Endo M, Yamaguchi S, Nanri K, Fujioka T. Parametric studies on improved laser cutting performance of magnesium alloy with two flow nozzles. *Japanese J of Applied Physics.* 2004; 43(8A):5347-5351.
- [9] Scintilla LD, Tricarico L. Experimental investigation on fiber and CO₂ inert gas fusion cutting of AZ31 magnesium alloy sheets. *Optics & Laser Technology.* 2013; 46:42-52.
- [10] Shigematsu I, Saito N, Nakanishi M, Mabuchi M, Matsuyama H, Nakamura M. Laser cutting of AZ31 magnesium alloy sheet. *J of Japan Institute of Light Metals.* 2000; 50(9):446-450.